Nonlinear polarization rotation-induced pulse shaping in a stretched-pulse ytterbium-doped fiber laser*

Bai Dong-Bi(白东碧), Li Wen-Xue(李文雪)†, Yang Kang-Wen(杨康文), Shen Xu-Ling(沈旭玲), Chen Xiu-Liang(陈修亮), and Zeng He-Ping(曾和平)

State Key Laboratory of Precision Spectroscopy, East China Normal University, Shanghai 200062, *China*

(Received 13 February 2014; revised manuscript received 24 March 2014; published online 10 August 2014)

We report on controllable pulse shaping in a Yb-doped stretched-pulse fiber laser followed by a high-power chirped pulse amplifier. We demonstrate that the pulses after an extra-cavity grating pair change their intensity profile from Lorentz to Gaussian and then to sech^2 shapes by adjusting the intra-cavity polarization through a quarter-wave plate inside the fiber laser cavity. The laser pulses with different pulse shapes exhibit pulse-to-pulse amplitude fluctuation of $\sim 1.02\%$, while the sech^2-shaped pulse train is provided with a more stable free-running repetition rate as a result of the stronger self-phase modulation in the fiber laser cavity than Lorentz- and Gaussian-shaped pulse trains.

Keywords: fiber lasers, nonlinear optics, mode locking, pulse generators

PACS: 42.55.Wd, 42.65.–k, 42.60.Fc, 84.30.Ng **DOI:** 10.1088/1674-1056/23/10/104208

1. Introduction

Pulse-shaped waveforms are attractive for a variety of applications in communications, transient detection and precision spectroscopy.[1,2] Meanwhile, stretched-pulse fiber lasers mode-locked with nonlinear polarization rotation (NPR) have been generally acknowledged as an advantageous source for producing ultra-short pulses with long-term stability.[3–5] It was discovered that the intra-cavity net dispersion plays a significant role in pulse evolution inside the fiber cavity in an NPR mode-locked fiber laser.[6–8] Moreover, the NPR effects are of crucial importance for determining the pulse dynamics.[9,10] Different intra-cavity laser polarizations could result in different mode-locking states with distinct optical features.[11,12] The influence of laser polarization rotation on pulse shape of the stretched-pulse fiber laser has been rarely reported so far, although the intrinsic mechanism of NPR mode-locking has been widely studied.

In this paper, we report on controllable pulse shaping in a high-power femtosecond fiber laser system consisting of an NPR mode-locked ytterbium-doped fiber laser oscillator, a double-cladding ytterbium-doped fiber amplifier, and pulse dechirping device with two extra-cavity fused-silica transmission gratings. Autocorrelation traces of the dechirped laser pulses could be changed among Lorentz, Gaussian, and sech^2 shapes by adjusting the intra-cavity laser polarization through rotating the quarter-wave plate (QWP) inside the fiber laser oscillator. The sech^2-shaped mode-locking state is influenced by larger intra-cavity self-phase modulation that facilitated a more stable free-running repetition rate than Lorentz and Gaussian mode-locking states.

2. Experimental setup and results

A schematic diagram of the experimental layout is presented in Fig. 1(a). The ring Yb-doped fiber laser cavity is constructed with a typical NPR configuration by using 80-cm Yb-doped fiber (YbDF350, OFS), $\sim$ 2.7-m standard single-mode fiber (SMF), and a free-space section. The free-space section includes wave plates, Faraday isolator, polarization-dependent beam splitter (PBS), and a pair of reflection gratings (600 lines/mm) separated by $\sim$ 6.1 cm. The total group-delay dispersion and third-order dispersion estimated in our fiber laser cavity are ~ 0.006 ps^2 and ~ 0.001 ps^3 respectively. As a result, the fiber laser can be mode-locked to deliver break-free and self-started pulses with an uncompressed pulse width of $\sim$ 2 ps. The 976-nm laser diode (LD) can supply $\sim$ 400-mW maximum pump power. It should be noted that in our experiment, we set the laser oscillator in an assembled windshield and install it on a negative stiffness vibration isolator table (100BM-4, Minus K) to prevent the undesired air fluctuation and mechanical vibration. In addition, we adopt a temperature feedback module (TEC control chip: ADN8830) in the self-developed laser diode driver circuit that adjusts the long-term temperature stability to 0.01 °C, and all our experiments are done in the standard optical laboratory with a tem-

*Project supported by the National Natural Science Foundation of China (Grant Nos. 11274115 and 10990101), the National Key Project for Basic Research of China (Grant No. 2011CB808105), the National Key Scientific Instrument Project, China (Grant No. 2012YQ150092), the Natural Science Foundation of Shanghai, China (Grant No. 11ZR1410900), and the Innovation Program of Shanghai Municipal Education Commission, China (Grant No. 2014Z10269011).

†Corresponding author. E-mail: wxli@phy.ecnu.edu.cn

© 2014 Chinese Physical Society and IOP Publishing Ltd

perature drift control to 0.1 °C.

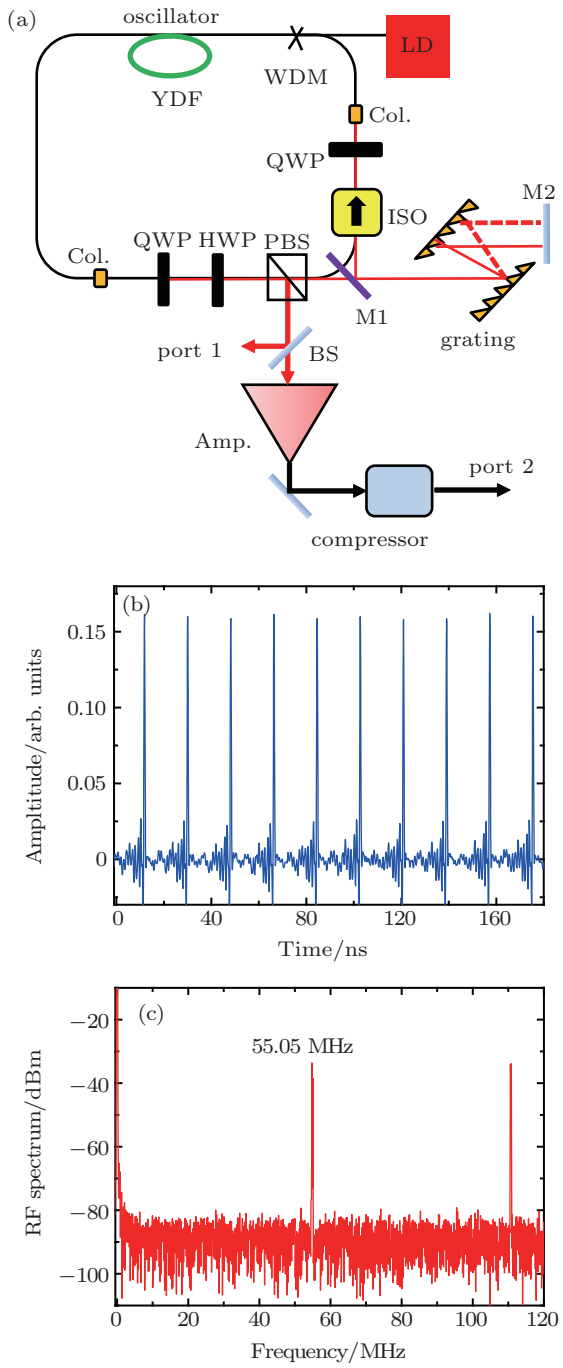


Fig. 1. (color online) (a) Experimental setup, (b) laser pulse train, and (c) RF spectrum of the fiber laser. WDM: wavelength division multiplexer, PBS: polarization beam splitter, M: mirror, Col.: collimator, ISO: isolator, YDF: Yb-doped fiber, QWP: quarter-wave plate, HWP: half-wave plate, LD: laser diode, and Amp.: amplifier.

Under a pump power of 180 mW, the average output power of the mode-locked pulses from Port 1 as marked in Fig. 1(a) is measured to be ∼ 27 mW. We detect the output pulse train from the fiber laser oscillator by using a fast photo-detector with a bandwidth of 1.5-GHz and record the signal by a digital oscilloscope with a bandwidth of 2.5-GHz (DSO9254A) and a radio-frequency (RF) spectrum analyzer (0.9 kHz∼ 3 GHz, N9010A) as shown in Figs. 1(b) and 1(c). The picosecond laser pulses are further power-scaled up to ∼ 20 W with a fiber amplifier of 1.5-meter-long large-mode-area Yb-doped double-cladding photonic-crystal fiber (YDCF), and then they are compressed down to ∼ 130 fs by a pair of transmission gratings (1200 lines/mm).[13] As shown in Fig. 2, the slope efficiency of the YDCF power amplifier reaches up to 70%.

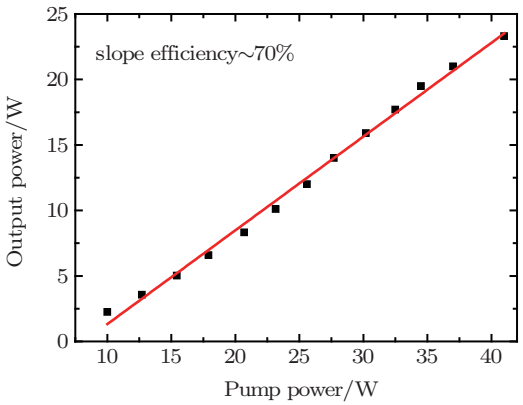


Fig. 2. (color online) The measured slope efficiency of the large-mode-area YDCF power amplifier.

We check the mode-locked pulse profiles by using the standard autocorrelation measurement after the YDCF amplifier and pulse-dechirping grating pair. An intriguing change of the output pulse profile is observed by rotating the quarter wave-plate (QWP) before the input collimator. When the QWP is set at discrete degrees of 94°, 100°, and 270°, the full-widths at half-maximum (FWHMs) of the chirped pulses from port 1 as marked in Fig. 1(a) are measured to be 3.52, 3.71, and 3.34 ps respectively. However, it is difficult to fit the pulse profiles of the fiber oscillator with some particular temporal shapes due to temporal deformation originating from the intra-cavity dispersion. Otherwise, with extra-cavity pair gratings, the pulses are dechirped and their intensity profiles can be well fitted by different line shapes. We carry out the nonlinear curve fitting to the data with some feasible line shapes and choose a line shape with a minimum deviation to optimally characterize the experimental results based on the value of adjusted coefficient of determination (which is abbreviated as adj. R^2) obtained from the statistical process. Consequently, the dechirped pulses at the QWP degrees of 94°, 100°, and 270° are best fitted by Lorentz, Gaussian, and sech^2 shapes with calculated pulse widths of 136, 187, and 165 fs, and adj. R^2 values of 0.99445, 0.99797, and 0.99830 respectively. Figures 3(a)–3(c) show the autocorrelation traces of the corresponding dechirped pulses from port 2 as marked in Fig. 1(a). In Figs. 3(a)–3(c) the black dots represent the measured data points and the solid lines denote the optimum fit pulse profiles. In order to enhance the contrast between the optimally fitted Gaussian and sech^2 pulses in our experiment,

we depict the sech^2 and Gaussian fit to the data in Figs. 3(b) and 3(c) in dashed lines, where the strong difference manifests itself in the steepness on the tails in both figures. Thus it is convincing to say that the Gaussian profile exhibits stronger explanatory power than the sech^2 profile for data in Fig. 3(b) and *vice versa* in Fig. 3(c).

Note that the pulse durations measured by autocorrelation are comparable to each other for all the dechirped pulses and the pulse width difference is mainly caused by the deconvolution factors. The corresponding laser spectra at the three QWP degrees before and after the amplifier are shown in Figs. 3(e)–3(f), indicating distinctive features of different states.

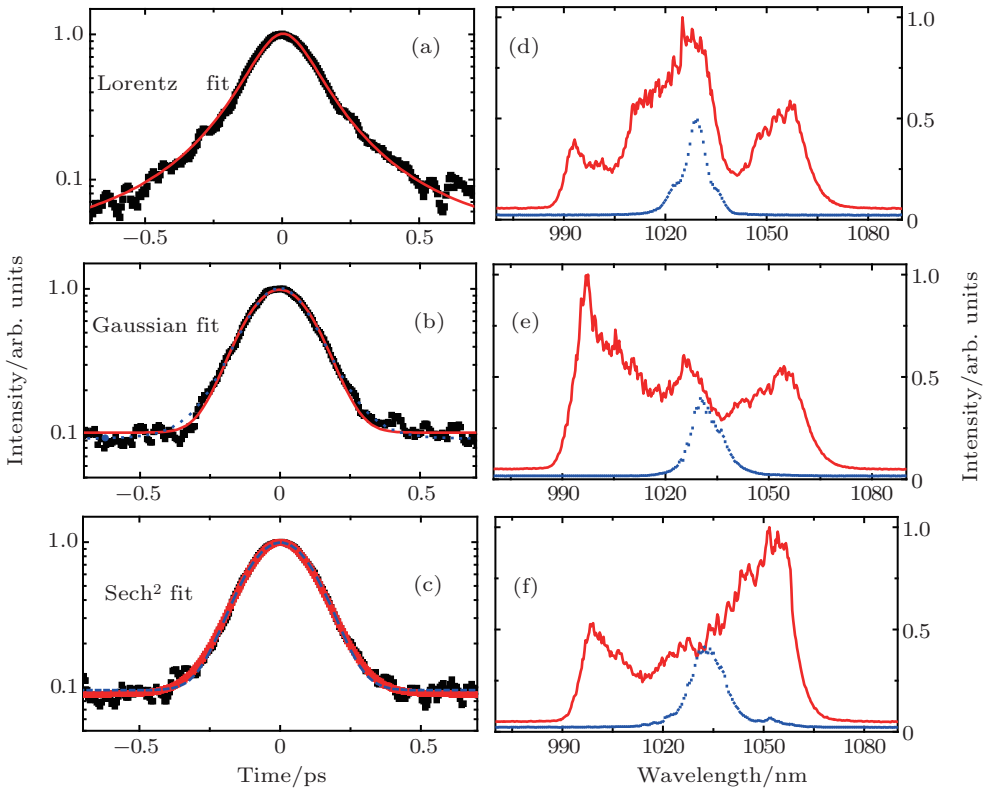


Fig. 3. (color online) (a)–(c) The autocorrelation traces of the dechirped pulses measured at the quarter-wave plate degrees of 94°, 100°, and 270° respectively. Black dots: recorded data points; red lines: optimum fitted pulse profiles for each type; dashed lines in panels (b) and (c) for sech^2 and Gaussian fit; (d)–(f) The corresponding laser spectrum for the pulses at quarter-wave plate degrees of 94°, 100°, and 270° respectively, before (solid lines) and after (dotted lines) the fiber amplifier.

In addition, we employ the second harmonic generation (SHG) frequency resolved optical gating (FROG) to measure the dechirped pulses and further discriminate their pulse shapes. As briefly depicted in Fig. 4(a), we divide the input pulses with a central wavelength of 1030 nm into two equivalent beams which undergo a non-collinear optical scheme and recombine and are frequency-converted at a β-barium borate (BBO). The attained visible light with a central wavelength of 515 nm is then coupled into a fiber spectrometer (HR4000, Ocean Optics) for the measurement of FROG trace under 400 iterations. The results when setting the quarter-wave plate degrees to be 94°, 100°, and 270° are demonstrated in Figs. 4(b)–4(d), Figs. 4(e)–4(g), and Figs. 4(h)–4(j) respectively. As observed from the comparisons, the three states exhibit distinguishable traces and the retrieve pulse temporal profiles in Figs. 4(d), 4(g), and 4(j) were optimally fitted by Lorentz, Gaussian and sech^2 shapes with FWHM of 150, 161, and 195 fs, and adj. R^2 value of 0.98223, 0.98027, and 0.97345 respectively, which are in good agreement with the results from standard autocorrelation measurements. It is worth mentioning that the errors between the measured and retrieved traces in the three measurements are all below 3×10^{-3} and the phase information shown herein confirms the well-managed chirp characteristics in our laser system.

To further describe this NPR-induced pulse shaping phenomenon, we investigate the relationship between the pump power and pulse shaping property by recording the pulse autocorrelation traces under the successive increasing of pump power of 70 mW, 180 mW, and 300 mW, respectively. The results are shown in Fig. 5, from which we discover that the optimally fitted pulse profiles will remain the same pattern as long as the angle of the QWP is fixed. However, the enhanced pump power can mostly provide a stronger nonlinear effect on the laser cavity and lead to the higher order chromatic dispersion of the medium material, and thereby result in the more severe distortion of autocorrelation curve that may affect the FWHM of the fitted pulse shape. Specifically, the FWHMs of the Lorentz, Gaussian, and sech^2 pulses fluctuate by 109 fs–120 fs, 153 fs–178 fs, and 148 fs–192 fs within the tuning range of the pump power.

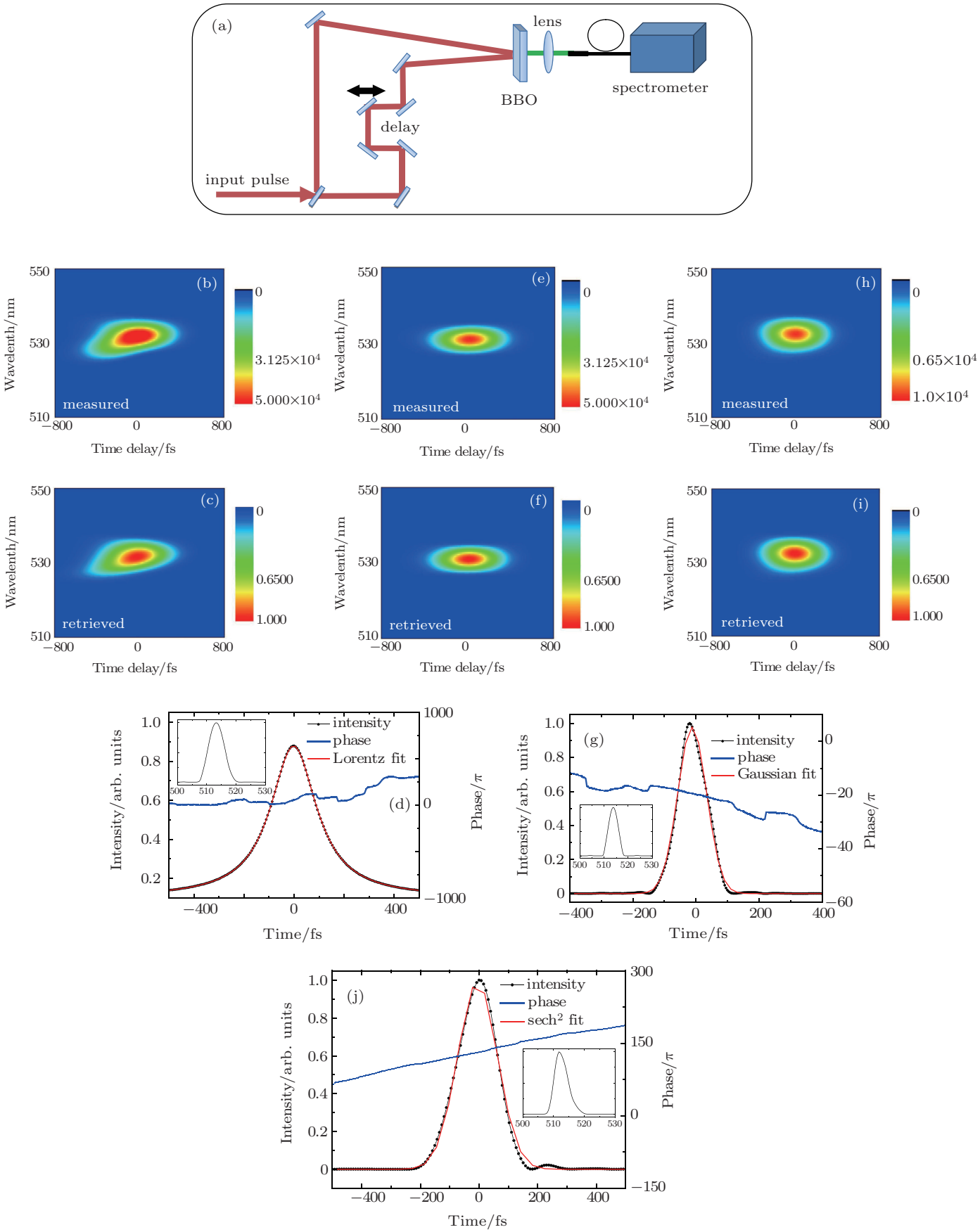


Fig. 4. (color online) (a) Experimental setup of FROG detection. (b)–(c), (e)–(f), (h)–(i) The measured and retrieved FROG traces of the dechirped pulses at the quarter-wave plate degrees of 94°, 100°, and 270° respectively. (d), (g), (j) The retrieved pulse temporal profile (dotted line) and their optimum fitted pulse profile (solid lines), and phase (middle curve) properties of the dechirped pulses at the quarter-wave plate degrees of 94°, 100°, and 270° respectively. Insets show the retrieved spectra.

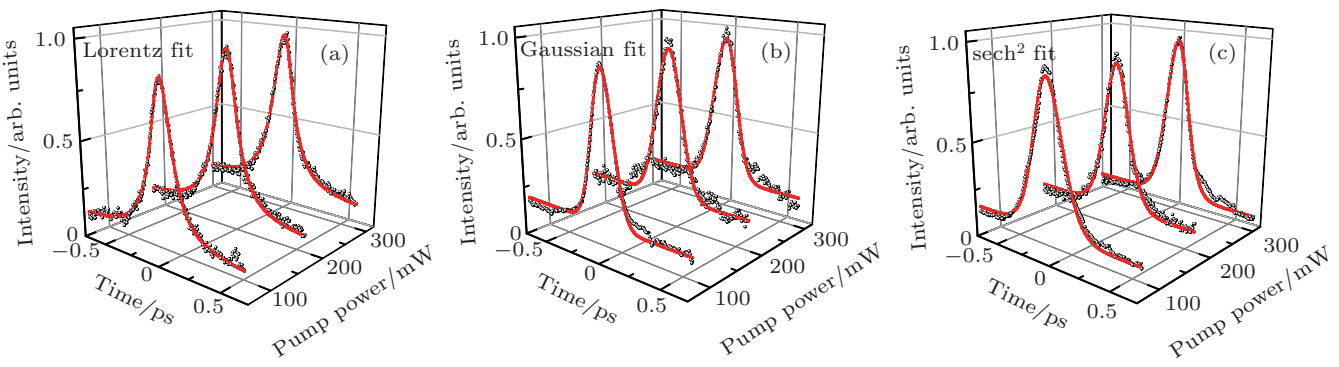


Fig. 5. (color online) (a)–(c) The autocorrelation traces of the dechirped pulses measured at the quarter-wave plate degrees of 94°, 100°, and 270° respectively, each under increasing pump power of 70 mW, 180 mW, and 300 mW. Dotted lines: recorded data points, solid lines: fitted pulse profiles for each type.

In order to explain the significance of the QWP in determining different pulse profiles, we investigate the pulse evolution in a single-mode fiber by the nonlinear Schrödinger equation (NLSE) as follows:[14]

$$\frac{\partial A(z,t)}{\partial z} = \mathrm{i}\gamma|A(z,t)|^2A(zt) - \frac{\alpha}{2}A(z,t) - \beta_1\frac{\partial A(z,t)}{\partial t} - \frac{\mathrm{i}\beta_2}{2}\frac{\partial^2 A(z,t)}{\partial t^2}.$$

Here, $A(z,t)$, α, β_1, β_2, and γ represent the function of slowly varying pulse envelope, the attenuation coefficient in the medium, the first-order propagation constant, the second-order coefficient of fiber group velocity dispersion (GVD), and the nonlinear coefficient of the fiber respectively. Thus the first and the second terms on the right-hand side of the above equation indicate the nonlinear optical effects and the losses exerted on the pulses when they propogate through the fiber, while the remaining two terms reveal the chromatic dispersion proprieties of the fiber. In the mode-locking technique of NPR, the role of the QWP mainly acts on the nonlinear optical proprieties of the pulses: to be specific, in combination with other wave plates, the QWP makes the linearly polarized light in laser cavity exhibit an elliptically polarized state that facilitates the nonlinear polarization rotation effects when the light undergoes the nonlinear Kerr medium, i.e., the fiber. This causes the central parts and the front-rear parts of the pulses in different polarization directions and thereby achieves the saturable absorbing effect to mode-lock the fiber laser device. Moreover, the intra-cavity PBS and QWP together permits a self-phase modulation (SPM)-induced spectral broadening and spectral filtering in the laser oscillator to deliver pulses in different line shapes. Specifically, by changing the angle of the QWP, the PBS can select the light components correspondingly in a wavelength-dependent way and they act as a tunable bandpass filter that allows only some specific spectral components of one polarization state to be reflected out of the cavity.[15] As a result, pulse components emitted by spectral filtering around the central region of the SPM spectrum (region A as marked in Fig. 6) form the output pulse of Lorentz shape as they possess the maximum slope efficiency with respect to the instantaneous frequency change with time for the SPM-broadened spectrum. Similarly, spectral filtering in region C as marked in Fig. 6 results in transform-limited pulses of Gaussian shape because of the minimum slope efficiency and the residual part of the SPM spectrum corresponds to the pulses of sech^2 autocorrelation trace, which represents a transform mode-locking state between Lorentz and Gaussian shapes. Besides, although the laser spectrum is narrowed by the fiber amplifier due to the finite gain bandwidth of the YDCF, each of the three states is still distinguishable. Thus the mode-locking states of the fiber oscillator herein are characterized by different dechirped pulse shapes as well as their distinctive laser spectrum.

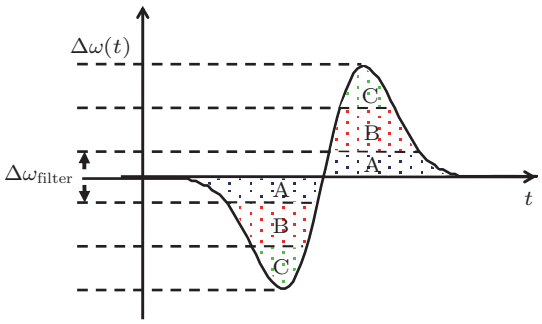


Fig. 6. (color online) Illustration of the instantaneous frequency change $\Delta\omega$ versus time t for the SPM-broadened spectrum. In the regions A, B, and C, spectral filtering of the SPM spectrum produced Lorentz, sech^2 and Gaussian-shaped pulses respectively.

Moreover, we record the changes of pulse shape at a series of QWP rotation angles. Figure 7 shows the measured pulse shapes, dechirped pulse widths as well as the oscillator output powers at different QWP degrees. The dechirped pulse exhibits a Lorentz shape as the QWP degree varies from 84°

to 96°, and then switched to a Gaussian shape at the QWP degrees from 98° to 105°. After being cut off by an unlocked range, the fiber laser resumes mode-locking with sech^2-shaped pulses as the QWP changes from 240° to 282°. Besides, in the process of adjusting QWP in the mode-locking range, the output power is maintained at $\sim$ 27 mW with negligible changes, while it suddenly jumped to $\sim$ 53 mW as the fiber laser is operated in unlocked continuous-wave (CW) state. Note that in our experiment all the data are measured by merely rotating the QWP clockwise while keeping the other experimental conditions unchanged. In this case, we find only two successive mode-locking regimes as indicated in Fig. 7. All the mode-locking states with their particular pulse shapes and laser spectra are reproducible. However, when the pump power or the degrees of the other two wave-plates are changed, the relationship between the QWP degree and laser output property should be updated. There exists a transition from Lorentz to Gaussian pulses when the QWP degree is $\sim$ 97°. In this case, a large pulse amplitude fluctuation is observed on the oscilloscope and the spectra before and after the amplifier change quickly and dramatically, indicating the appearing of mode-locking state transition. Moreover, as the fiber laser is mode-locked in the stable region, the pulse is self-stabilized with the intensity fluctuation as small as $\sim$ 1.02%, which is independent of pulse shape.

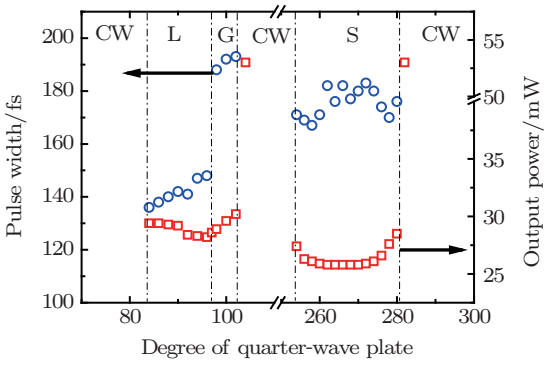


Fig. 7. (color online) The mode-locking states of the fiber laser including pulse width (blue circle) and output power (red square) at different QWP degrees. CW: unlocked continuous-wave lasing; L, G, and S stand for Lorentz, Gaussian and sech^2 shaped pulses respectively.

To further characterize these three mode-locking states, we measure the free-running laser repetition rate and their time evolution, at typical QWP degrees of 94°, 100°, and 270° respectively, by a digital frequency counter with 1-s gate (Agilent 53131A). The results are shown in Fig. 8. The three different states exhibit similar characteristics with a slow frequency drift accompanied by a fast frequency variation. The repetition rate drifts within half an hour are measured to be 32, 30, and 17 Hz for the Lorentz, Gaussian, and sech^2 shaped pulses respectively, with a similar fast frequency variation of $\sim$ 0.15 Hz. Interestingly, the sech^2 pulses show a drifting frequency approximately half of those of the other two shaped pulses. In order to confirm this distinct performance, we measured the laser repetition rate at several QWP degrees within the sech^2-pulse regime after a few days, and obtained similar results. Actually, we have installed the reflection mirror (M_2) in a translation stage to adjust the cavity length. It is found that the oscillating spectrum of sech^2 state changes against the adjustment, while no clear spectral changes are observed for the other two shaped pulses. The inset of Fig. 8(c) shows the variations of spectra when the cavity length is increased by 1.0 cm and 2.0 cm respectively. Based on the shock isolation measurement we have adopted in the laser system, it is convinced that the environmental and other conditions exert negligible effects on the variation of the repetition rate. Therefore, we attribute the stable repetition rate of the sech^2 state to a stronger SPM which compensates for fiber cavity-length variation with considerable spectral changes.

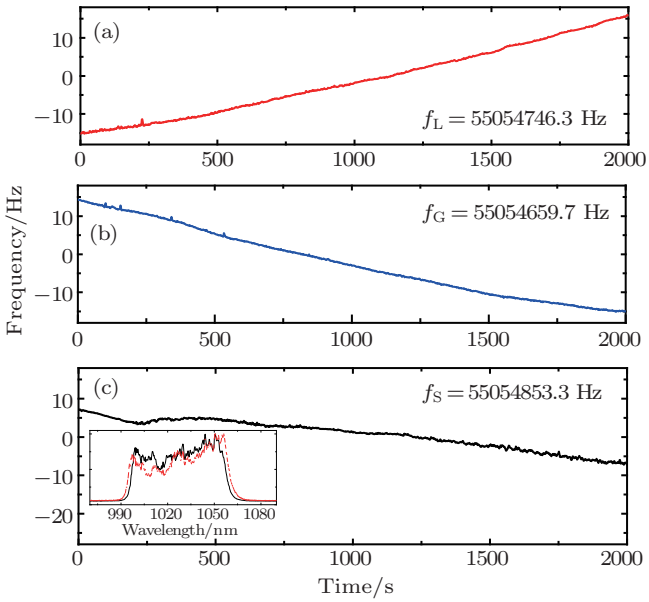


Fig. 8. (color online) The free-running repetition rates for (a) Lorentz, (b) Gaussian and (c) sech^2 pulses. The inset shows the laser spectra measured with cavity length increased by 1 cm (solid line) and 2 cm (dotted line) respectively.

3. Summary

In summary, we demonstrated a high-power stretched-pulse Yb-doped fiber laser system that can be operated at different mode-locking states of Lorentz, Gaussian, or sech^2 autocorrelation traces by tuning the intra-cavity polarization state. Particularly, the sech^2 pulses exhibit a more stable free-running repetition rate than the other pulses due to corresponding strong self-phase modulation in the fiber laser cavity. The laser pulses with different shapes are demonstrated to exhibit similar intensity fluctuations. The observed relationship between pulse shapes and intra-cavity laser polarization is ben-

eficial to further investigating NPR mode-locked fiber lasers, and long-term stable operation of high-power fiber lasers is anticipated to benefit a variety of applications in precision spectroscopy.

References

[1] Weiner A M, Heritage J P and E. M. Kirschner 1988 *J. Opt. Soc. Am. B* **5** 1563

[2] Schibli T R, Hartl I, Yost D C, Martin M J, Marcinkevicius A, Fermann M E and Ye J 2008 *Nat. Photon.* **2** 355

[3] Kieu K, Renninger W H, Chong A and Wise F W 2009 *Opt. Lett.* **34** 593

[4] Yan M, Li W X, Yang K W, Bai D B, Zhao J, Shen X L, Ru Q T and Zeng H P 2012 *Opt. Lett.* **37** 3021

[5] Ilday F, Buckley J, Kuznetsova L and Wise F W 2003 *Opt. Express* **11** 3550

[6] Glandorf L, Johnson T A, Kobayashi Y and Diddams S A 2011 *Opt. Lett.* **36** 1578

[7] Song Y J, Jung K Y, and Kim J W 2011 *Opt. Lett.* **36** 1761

[8] Baumgartl M, Ortaç B, Limpert J and Tünnermann A 2012 *Appl. Phys. B* **107** 263

[9] Renninger W H, Chong A and Wise F W 2012 *IEEE J. Sel. Top. Quantum Electron.* **18** 389

[10] Gee S, Quinlan F, Ozharar S and Delfyett P J 1995 *IEEE J. Sel. Top. Quantum Electron.* **31** 591

[11] Shen X L, Li W X, Yan M and Zeng H P 2012 *Opt. Lett.* **37** 3426

[12] Salhi M, Leblond H, and Sanchez F 2003 *Phys. Rev. A* **67** 013802

[13] Yan M, Li W X, Yang K W, Zhou H, Shen X L, Zhou Q, Ru Q T, Bai D B and Zeng H P 2012 *Opt. Lett.* **37** 1511

[14] Agrawal G P 1989 *Nonlinear Fiber Optics* (New York: Elsevier (Singapore) Pte Ltd.) pp.199–206

[15] Lehneis R, Steinmetz A, Jauregui C, Limpert J and Tünnermann A 2012 *Opt. Lett.* **37** 4401